Soft Matter

PAPER

View Article Online
View Journal | View Issue

Cite this: *Soft Matter*, 2017, **13**, 1455

Clathrin polymerization exhibits high mechano-geometric sensitivity†

Ehsan Irajizad,[a] Nikhil Walani,[a] Sarah L. Veatch,[b] Allen P. Liu[c] and Ashutosh Agrawal*[d]

Received 21st November 2016,
Accepted 2nd January 2017

DOI: 10.1039/c6sm02623k

rsc.li/soft-matter-journal

How tension modulates cellular transport has become a topic of interest in the recent past. However, the effect of tension on clathrin assembly and vesicle growth remains less understood. Here, we use the classical Helfrich theory to predict the energetic cost that clathrin is required to pay to remodel the membrane at different stages of vesicle formation. Our study reveals that this energetic cost is highly sensitive to not only the tension in the membrane but also to the instantaneous geometry of the membrane during shape evolution. Our study predicts a sharp reduction in clathrin coat size in the intermediate tension regime (0.01–0.1 mN m^{-1}). Remarkably, the natural propensity of the membrane to undergo bending beyond the Ω shape causes a significant decrease in the energy needed from clathrin to drive vesicle growth. Our studies in mammalian cells confirm a reduction in clathrin coat size in an increased tension environment. In addition, our findings suggest that the two apparently distinct clathrin assembly modes, namely coated pits and coated plaques, observed in experimental investigations might be a consequence of varied tensions in the plasma membrane. Overall, the mechano-geometric sensitivity revealed in this study might also be at play during the polymerization of other membrane remodeling proteins.

1 Introduction

How the physical properties of the membrane control membrane–protein interactions that lead to structural remodeling during numerous cellular processes is a fundamental open question in biology.[1] One such vital and evolutionary conserved physical process is clathrin-mediated endocytosis (CME), which living cells use to uptake extracellular molecules through the formation of clathrin-coated pits (CCPs) and subsequent internalization into intracellular vesicles.[2,3] CME is important for the exchange of lipids and proteins between the plasma membrane and organelles and is critical for maintaining the organization of the plasma membrane and regulating signal transduction pathways. While clathrin was discovered several decades ago, how clathrin polymerizes and remodels membranes is still a subject of active investigation.[4]

For example, recent studies have demonstrated the impact of a key physical parameter, tension in the plasma membrane, on CME. In a low-tension environment, vesicle formation in mammalian cells is primarily driven by clathrin polymerization and is actin-independent.[5–7] In contrast, in a high-tension environment, either due to the polarized nature of cells or due to mechanical manipulation of cells, vesicle formation becomes actin-dependent.[8,9] Along similar lines, CME in yeast cells, which experience high membrane tension due to large internal turgor pressure, is known to be actin-dependent.[5,10–13] The impact of cortical tension on the CCP dynamics has also been shown within single cells.[14] This has led to a natural question as to how tension impacts CCP dynamics.

The *in vitro* studies by Saleem *et al.* showed that vesicles subjected to increased tension exhibited reduced clathrin polymerization.[15] Tan *et al.* showed that CCPs in cells subjected to increased cell spreading size exhibit increased short-lived CCPs and initiation rate.[16] These experimental studies are complimented by the modeling work of Walani *et al.*, which suggests that an increase in tension should lead to a smaller clathrin coat in order to match experimentally observed shapes in mammalian and yeast cells.[17] In addition, stochastic models have provided fundamental insights into clathrin self-assembly[18,19] and dynamic rearrangements in clathrin lattices.[20–22] In particular, curvature generation by indentation has been shown to promote solid to fluid phase transition in a planar clathrin lattice.[21]

While these studies have provided fundamental insights into the different aspects of CCP dynamics, how membrane curvature and tension simultaneously regulate clathrin polymerization

[a] *Department of Mechanical Engineering, University of Houston, Houston, TX, USA*
[b] *Department of Biophysics, University of Michigan, Ann Arbor, MI, USA*
[c] *Department of Mechanical Engineering, University of Michigan, Ann Arbor, MI, USA*
[d] *Department of Mechanical Engineering, University of Houston, Houston, TX, USA. E-mail: ashutosh@uh.edu*

† Electronic supplementary information (ESI) available. See DOI: 10.1039/c6sm02623k

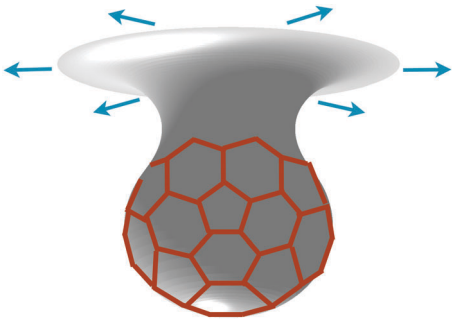

Fig. 1 The focus of the study is to predict the clathrin coat (red lattice) area that would polymerize under different membrane tension conditions. To this end, we employ the classic Helfrich theory to estimate the instantaneous energy that the clathrin monomers would have to provide during the shape evolution to drive vesicle growth.

during vesicle growth is not yet well understood. Here, we use continuum mechanics to estimate the polymerization energy needed to bend the membrane during shape evolution under different homeostatic tension conditions (Fig. 1). Our study reveals that the vesicle growth is associated with a highly nonlinear energy demand which clathrin has to meet in order to bend the membrane. Remarkably, the energetic demand reaches its peak at a critical geometric point beyond which curvature energy contributes to vesicle growth and necking. Our study reveals a reduction in the CCP size in the intermediate tension regime and formation of coated plaques in a high tension regime. The former finding is supported by our experimental studies in mammalian cells.

2 The basic setup

We model the bilayer as a 2D surface and use the well-known Helfrich theory to model clathrin-induced membrane remodeling. The strain energy for the membrane is given by $W = \kappa(H - C)^2 + \bar{\kappa}K$, where H is the mean curvature, K is the Gaussian curvature, C is the effective spontaneous curvature imposed by the clathrin coat, and $\{\kappa, \bar{\kappa}\}$ are the bending moduli.[23–27] Since we do not model topological changes, the second term in the energy does not contribute to the energetics of the shape evolution due to the Gauss–Bonnet theorem. We do not take into account the effects of other membrane remodeling proteins such as actin and BAR (in the case of yeast cells) to isolate the impact of tension and geometry on clathrin polymerization. Such an insight is valuable to understand the extent of clathrin-induced membrane remodeling in a high tension regime. In addition, since membranes only undergo a minimal areal dilation of 2–3%, we impose areal incompressibility.

We explore equilibrium solutions in the axisymmetric domain parametrized by the meridional arc length s and the azimuthal angle θ. For this system the equilibrium equations reduce to

$$\kappa\Delta(H - C) + 2\kappa(H - C)(2H^2 - K) - 2\kappa H(H - C)^2 = 2\lambda H \quad (1)$$

and

$$\lambda' = -W' \quad (2)$$

where λ is the surface tension, $\Delta(\cdot)$ is the surface Laplacian and $(\,)'$ is the partial derivative with respect to the arclength. We solve these equations along with the geometric equations

$$r'(s) = \cos\psi \quad \text{and} \quad z'(s) = \sin\psi. \quad (3)$$

and

$$\psi' = 2H - \frac{\sin\psi}{r} \quad (4)$$

to compute the equilibrium shapes. Above, $r(s)$ is the radius from the axis of revolution, $z(s)$ is the elevation from a base plane and $\psi(s)$ is the angle which the tangent makes with the radial vector.

In the coated domain, we assume that the clathrin coat imposes a spontaneous curvature $C_0 = 1/R_0$, where $R_0 = 50$ nm is the preferred radius of curvature of the clathrin coat,[28,29] and an effective membrane stiffness ten times higher than that of the uncoated membrane.[30] To model these spatial variations, we prescribe

$$\frac{C}{C_0} = \frac{1}{2} - \frac{\tanh(\beta(s - s_0))}{2}, \quad (5)$$

and

$$\frac{\kappa}{\kappa_0} = 1 + \frac{9}{2}[1 - \tanh(\beta(s - s_0))] \quad (6)$$

where $\kappa_0 = 20k_BT$ is the bending modulus of the uncoated membrane, $\beta = 12$ is a constant that determines the sharpness of the tanh function and s_0 is the prescribed domain of the clathrin coat in terms of the arc length. The spatial variation in κ and C in the uncoated and coated domains for a typical vesicle geometry is shown in Fig. 2. As shown for the first time by Agrawal and Steigmann,[31] such a spatial heterogeneity in membrane properties can potentially lead to a variable surface tension field in the membrane.

We integrate the differential equations with the appropriate boundary conditions to compute the CCP shapes (Fig. 3). At the pole of the CCP, lying on the axis of revolution, we require $r = 0$, $\psi = 0$ and $L = r[\kappa(H - C)]' = 0$. The last condition, $L = 0$, where L represents the transverse shear force in the membrane, is associated with the requirement that there is no applied point load at the pole.[32] At the outer periphery, we impose $z = 0$, $\psi = 0$, and $\lambda = \lambda_0$, the prescribed tension in the membrane. We use the coat area of $4\pi R_0^2$ as the reference area. This corresponds to the maximum (100%) area that a coat can have at zero tension. We vary the coat area and compute the equilibrium shapes for a fixed resting tension in the membrane. In order to have a handle on the coat area, we switch to area as the independent variable. The procedure is presented in ref. 32. In addition, we use R_0 as the lengthscale to normalize the equations. As a consequence, the qualitative nature of our results is valid for any arbitrary radius preferred by the clathrin coat.

The mathematical framework mentioned above has been used extensively to investigate endocytosis and nanoparticle uptake[17,31,33–40] (for more studies on endocytosis of nanoparticles, see references in ref. 39). In this study, we use the same framework to simulate vesicle shapes but we ask a different question.

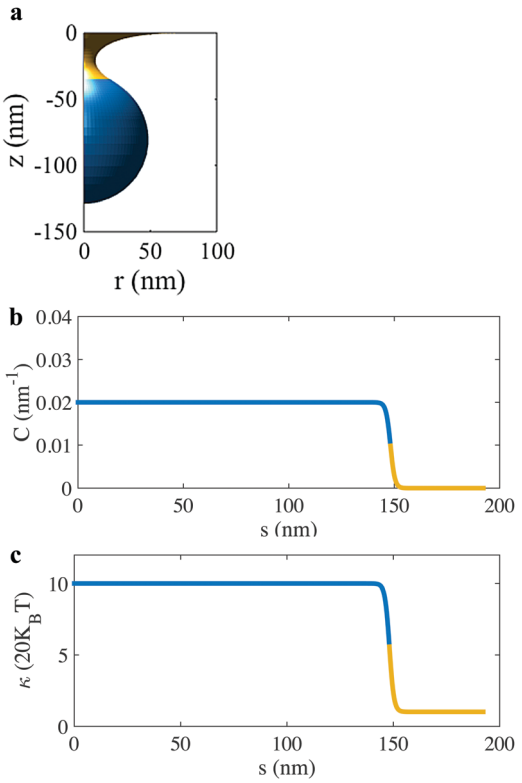

Fig. 2 Effect of the clathrin coat on the membrane properties. (a) A typical shape of a vesicle during shape evolution. The blue domain indicates the clathrin coated region. (b and c) The spatially varying spontaneous curvature and bending modulus fields for the vesicle geometry shown in (a).

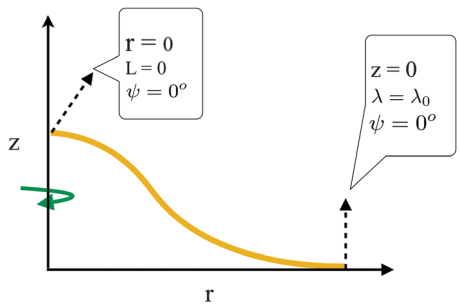

Fig. 3 The key variables and the boundary conditions employed in the axisymmetric model to compute vesicle geometry.

How much energy does clathrin impart to bend the membrane during shape evolution? In other words, if we start from a planar patch of membrane, how much energy do clathrin trikelions have to impart to bend the membrane and turn it into a bud. We can investigate this problem by computing the work done to go from a planar state to an invaginated state. This work comprises two components. The first is the energy required to bend the bare membrane. In the framework of Helfrich theory, this energy would be given by the integration of κH^2. The second contribution comes from pulling the membrane against the resting tension towards the endocytic site.

A simple thought experiment could provide additional insight into these energetic contributions. Let us assume that we start with a planar membrane at zero tension. Let us further assume that clathrin polymerizes onto the membrane and transforms it into a nearly spherical bud. In this scenario, $H = C$. If we compute the bending energy of the composite membrane–clathrin system, it is equal to zero. However, it does not imply that clathrin did not do any work in bending the membrane. In fact, the bending energy of a sphere is equal to $4\pi\kappa$, which is supplied by the clathrin coat. It is for this reason that we compute the bending energy of the uncoated membrane. A similar idea was employed in ref. 41 to compute the cost to form a vesicle. Since the resting tension is zero, no work is done for pulling the membrane with a surface area equal to $4\pi R_0^2$ towards the endocytic site (R_0 is the radius of the clathrin coat and $C = 1/R_0$).

We compute the energy for the entire shape evolution and then compute the rate of change of energy per unit clathrin coat area. This 'energy density ε' is the polymerization energy that the newly added clathrin coat is required to supply at any stage in order to further drive vesicle growth. If the polymerization energy of clathrin, ε_c, at any stage is equal to or greater than the required ε, clathrin can polymerize and bend the membrane. If not, clathrin polymerization and vesicle growth will stall. This approach differs from the notion of computing the average polymerization energy obtained from the ratio of the required bending energy $4\pi\kappa$ with the spherical coat area (as in ref. 41). Here, the polymerization cost is predicted as a function of the vesicle geometry during shape evolution.

3 Results

The key results, the required polymerization energy ε (rate of change of energy per unit clathrin coat area) computed during shape evolution at different resting tension values, are presented in Fig. 4. The total energy plots for the corresponding cases are presented in Fig. S1 (ESI†). The plots exhibit four different patterns. Fig. 4a presents ε in very low tension regimes – $\lambda_0 <$ 0.015 mN m^{-1}. First, ε increases at a rapid rate until clathrin reaches 6–7% coat area. Next, it increases at a reduced rate until it reaches a maximum around 60% coat area. Beyond this critical point, ε drops rapidly and plateaus in the rest of the area domain. This behavior reveals interesting physics associated with membrane geometry. Up to the critical point ($\sim$60% coat area), monotonically increasing polymerization energy is required to drive invagination. However, beyond this critical point, the geometry itself favors closure of the vesicle and as a result the energy required from clathrin undergoes a reduction. Thus, membrane geometry plays a critical role in determining the energetic input required from the protein to drive vesicle growth.

Fig. 4b shows the energy requirement in the next higher tension domain – 0.015–0.05 mN m^{-1}. Here, the plots exhibit similar behavior to that exhibited before up to the critical point ($\sim$70% coat area), which corresponds to an Ω shaped CCP. However, beyond the critical point, the vesicle undergoes a snapthrough instability and the curves undergo a sharp decline. This trend is a scaled-up version of the very low tension response. The effect of geometry is stronger, and the membrane

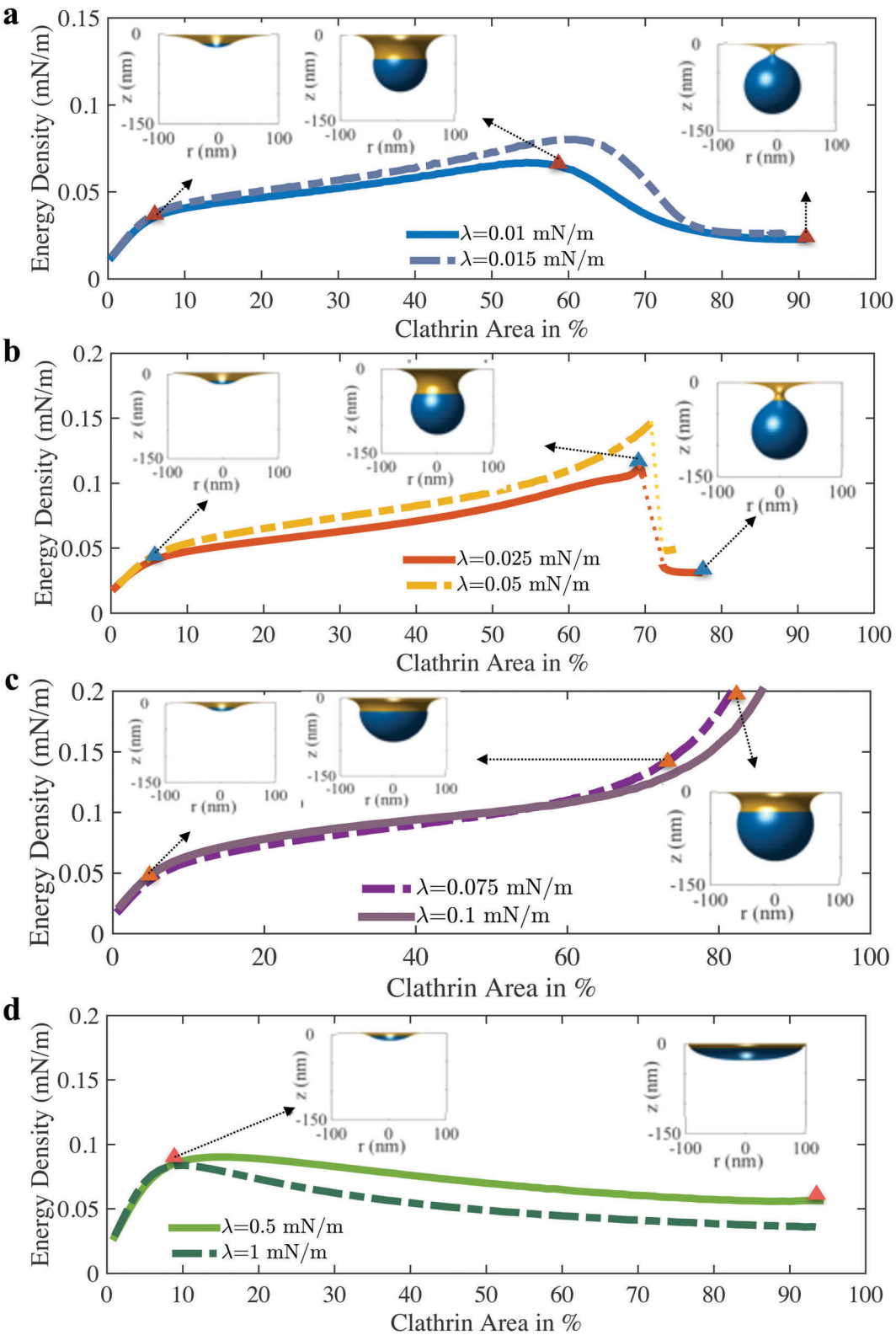

Fig. 4 Rate of change of energy with respect to clathrin coat area in different tension (λ) regimes (a–d). This is the required polymerization energy that clathrin should possess in order to drive vesicle growth. This energy density shows high sensitivity to both membrane geometry and tension. The insets show the bud morphology at the critical junctures during shape evolution. All the insets have the same axis allowing a direct comparison between bud profiles at different coat areas and membrane tension. The golden domain indicates the bare membrane and the blue domain indicates the clathrin-coated domain.

has a much higher propensity to undergo necking. In the next higher tension regime (0.075–0.1 mN m^{-1}), ε increases monotonically and smoothly up to 80% clathrin coat area (Fig. 4c). However, ε undergoes a rapid increase beyond 70% clathrin coat area, which corresponds to an Ω shaped CCP. Interestingly, in this regime, even an 80% clathrin coat area is only able to create a partial vesicle. For higher coat areas, intriguingly, no converged solutions are obtained. Our speculation is that for a higher coat area, there are two competing effects. While on one hand the vesicle wants to close up as in Fig. 4b, on the other hand, the coat size is large enough for the vesicle requiring the coat to go into the neck region. Since this would entail significant energetic cost due to curvature frustration, the vesicle does not achieve a closed geometry as in Fig. 4b and gets stalled in the Ω-shaped geometry. Finally, in the high tension regime, >0.1 mN m^{-1}, there is a trend reversal (Fig. 4d). The required polymerization energy (ε) first increases up to a critical point around 10% coat area and then decreases smoothly in the rest of the area domain. In this regime, due to very high tension, even 90% coat area is unable to drive vesicle growth and the membrane stalls at a very shallow CCP.

While the required polymerization energy plots show different trends, the corresponding CCP invagination depths show similar behavior in all the tension regimes (Fig. 5). The depth increases monotonically with an increase in the area and decreases with an increase in the tension. Only in the low tension regime, contrary to intuition, the depth decreases beyond 70% coat area. This effect most likely results from the closure of the vesicle which tends to pull the entire CCP towards the planar membrane.

So, what conclusions can be drawn about the size of the clathrin coat from the results presented in Fig. 4? If we assume that clathrin has a fixed polymerization energy ε_c, we can determine the maximum coat area corresponding to this value from the ε plots presented in Fig. 4. For example, clathrin is able to form nearly spherical coats in mammalian cells that have an estimated tension in the order of $\sim$0.01 mN m^{-1}.[41–43] Fig. 4a then shows that if clathrin has ε_c = 0.065 mN m^{-1}, it would be able to meet the highest energy demand and form a full spherical coat. If we assume that this polymerization energy remains constant in different mechanical environments, we can determine the clathrin coat area corresponding to $\varepsilon = \varepsilon_c$ = 0.065 mN m^{-1} at different tension values. This yields a plot of the clathrin coat area as a function of tension presented in Fig. 6a (red curve). The plot reveals a sharp decline in the clathrin coat area with an increase in the membrane tension. Remarkably, the coat area drops drastically by almost 95% until the tension of 0.2 mN m^{-1} is achieved. Beyond 0.2 mN m^{-1}, the coat area becomes insensitive to tension and remains constant.

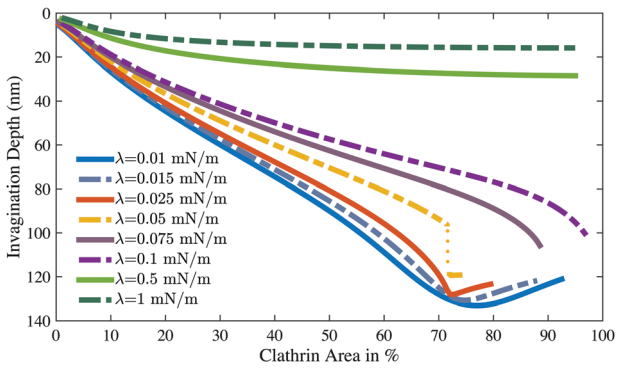

Fig. 5 CCP invagination depth obtained in different tension regimes for different clathrin coat domains. Under most scenarios, the depth increases monotonically. In a low tension regime, the vesicle retracts marginally due to necking and CCP closure.

To gain a deeper understanding into the relationship between the polymerization energy and the predicted coat area, we consider another scenario. We compute clathrin coat areas corresponding to a polymerization energy equal to 0.1 mN m^{-1}. The blue curve in Fig. 6a shows the coat areas for ε_c = 0.1 mN m^{-1}. Interestingly, the plot shows a very different trend compared to the red curve (corresponding to ε_c = 0.065 mN m^{-1}). For ε_c = 0.1 mN m^{-1}, the clathrin coat area first decreases rapidly up to 0.1 mN m^{-1} and reaches a value of $\sim$45%. Remarkably, it then begins to increase smoothly up to $\sim$0.35 mN m^{-1} and reaches a value of $\sim$90%. After $\sim$0.35 mN m^{-1}, the polymerization energy is higher than the required values suggesting that any arbitrary coat area greater than 100% can polymerize. However, in Fig. 6a, we cap the polymerized area to a maximum of 100% (dotted blue curve).

While the predicted clathrin coat area is sensitive to the polymerization energy that clathrin possesses, the maximum invagination depth of the CCP shows a robust trend. The invagination depths corresponding to the two curves in Fig. 6a are presented in Fig. 6b. In both the scenarios, the invagination depth monotonically decreases with an increase in tension. It is important to note that despite large variations in the coat areas in the medium to high tension regimes for the two cases, the invagination depths remain small and comparable. This reveals a tension-dependent decoupling between the polymerized coat area and the CCP invagination depth. In fact, prescribing a higher coat area (>100%) in the high tension regime for ε_c = 0.1 mN m^{-1} has a minimal impact on the invagination depth. Thus, our choice for capping the coat area to a maximum of 100% has no physical consequence on vesicle growth.

Our modeling results suggest that there is an inverse relationship between CCP size and tension in the low to intermediate tension regimes. It was shown previously that cells spread on large fibronectin micropatterned substrates had higher tension compared to small micropatterned substrates.[16] In order to directly observe CCP sizes on different sized micropatterned substrates, we performed superresolution imaging by stochastic optical reconstruction microscopy (STORM). Endogenously expressed clathrin heavy chain molecules were immunolabeled using X22 monoclonal anti-clathrin heavy chain and Alexa Fluor 647 conjugated antibodies (Abcam) and imaged and analyzed as described previously.[44,45] As shown in Fig. 7, CCPs were clearly larger in a cell on a small micropatterned substrate, consistent with our modeling results. Furthermore, the average correlation lengths computed from autocorrelation functions of the resultant superresolution localization data for the small and large micropatterns were 73 ± 4.2 nm and 54 ± 3.8 nm,[45] respectively,

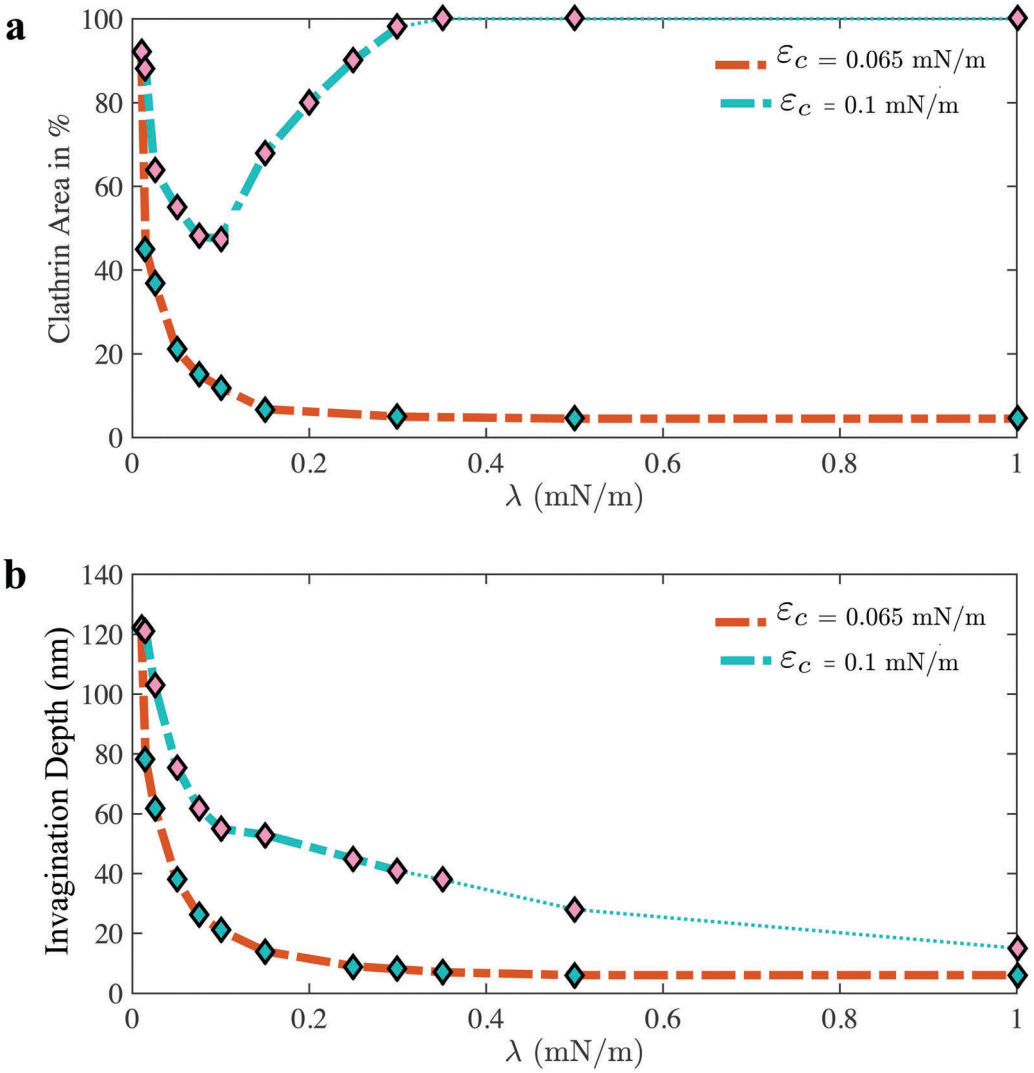

Fig. 6 (a) Predicted clathrin coat area as a function of membrane tension for two different clathrin polymerization energies ε_c. The predicted clathrin coat area decreases rapidly in the intermediate tension regime. For $\varepsilon_c \geq 0.1$ mN m^{-1}, our study predicts the formation of coated plaques (nearly planar CCPs) of arbitrary size in a high tension regime. Here, we cap the maximum area to 100% (dotted line). (b) Corresponding CCP invagination depths for the predicted clathrin coat area. Despite a vast variation in the clathrin coat areas for the two polymerization energies, CCP invagination depth shows a monotonic decline with an increase in membrane tension.

indicating a larger CCP size in cells with lower tension. These results support the modeling predictions.

4 Discussion

In this study, we have used the Helfrich theory to model the energetics of clathrin–membrane interaction. Our results reveal that the polymerization energy required to transform a planar membrane into a vesicle shows a highly nonlinear trend determined synergistically by both the geometry and the tension of the membrane. The study shows that the Ω shaped geometry of the CCP is a critical point, beyond which much less work is needed from clathrin to drive vesicle growth. This effect of geometry is reminiscent of the drop in the force observed during pulling of a tubule from a planar membrane or a vesicle.[17,46,47] In addition, our study shows that the coat size shows extreme sensitivity to membrane tension and decreases rapidly in the low to intermediate tension regimes. Finally, our study presents a counterintuitive finding that the clathrin coat size could reach arbitrarily large values in high tension regimes if clathrin possesses a polymerization energy of ~0.1 mN m^{-1}. However, despite the increased coat size, the CCP remains nearly flat (Fig. S2, ESI†).

The experimental findings in mammalian cells performed in this study show the predicted decrease in the CCP size in an increased tension environment. The *in vitro* study by Saleem *et al.*[15] also revealed a reduction in clathrin polymerization on vesicles subjected to hypoosmotic conditions. These experimental findings are aligned with the modeling predictions in the low to intermediate tension regimes. In our experimental setup, we were limited by the degree of cell spreading on the micropatterned substrates, and we found that cells were unable to reliably spread

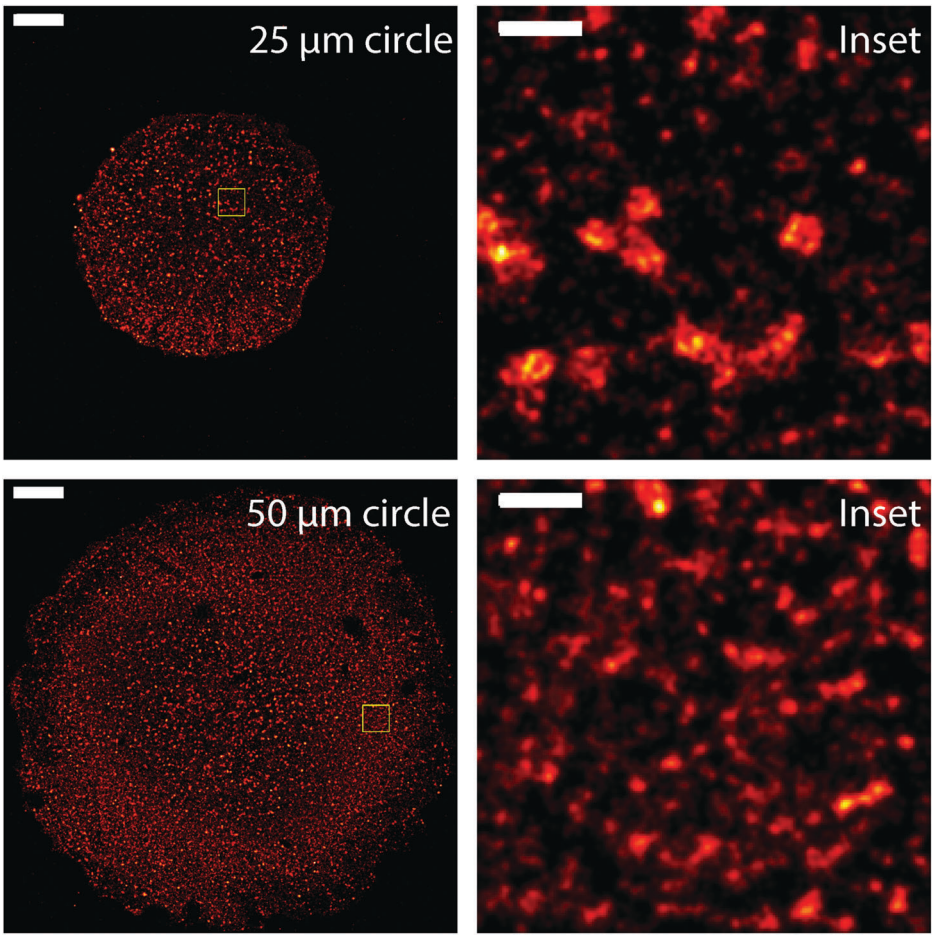

Fig. 7 Superresolution images of CCPs of retinal pigment epithelial cells on 25 micron (top) and 50 micron (bottom) circle micropatterns. Insets of the yellowed boxed regions are shown on the right. Images are blurred with 2D Gaussian at a radius of 50 nm and 20 nm for full and inset images, respectively. Scale bars are 5 micron and 500 nm for the full and inset images, respectively.

beyond 50 micron diameter circular patterns. Thus, while our other prediction that large shallow clathrin coats can form in a high tension regime is not observed in these experiments, planar or moderately curved clathrin structures called 'coated plaques' have been observed on the adhered surfaces of mammalian cells.[48,49] Since cell–substrate adhesion can inhibit membrane bending in a manner similar to high membrane tension, the two scenarios can have similar energetics, giving rise to coated plaques of arbitrary sizes. Our study, therefore, suggests that geometrical constraint coupled with adequate polymerization energy could be a cause of coated plaque formation. Overall, our work reveals the interplay between geometry and elasticity associated with membrane–protein interactions that could regulate the polymerization of other scaffolding proteins such as COPI, COPII, caveolins and BAR proteins.

We would like to note that the notion of spontaneous curvature and polymerization energy for clathrin should be interpreted in a more broader context. While clathrin is known to bend and polymerize on the membrane, its interaction with the membrane is also associated with the recruitment of several accessory proteins.[3,50,51] These proteins can potentially have a similar remodeling effect on the membrane and can alter the clathrin–membrane binding energy. As a result, the spontaneous curvature and the polymerization energy used in this study should be interpreted as effective parameters arising from a complex interplay between clathrin and the accessory proteins.

Lastly, our model assumes continuous polymerization of clathrin during vesicle growth. This mechanism is aligned with numerous experimental and modeling studies present in the literature.[16,17,31,35,36,52–54] However, the recent paper by Avinoam[4] reveals an alternative mechanism in which the entire clathrin coat first polymerizes on a nearly planar membrane and then undergoes geometric remodeling driving vesicle formation. The factors that regulate the clathrin coat size in this model are currently unknown. Furthermore, how membrane tension would inhibit clathrin polymerization on a planar membrane in this model remains to be seen and will be a subject of future study.

Acknowledgements

A. A. acknowledges support from NSF Grants CMMI 1437330 and CMMI-1562043. A. P. L. acknowledges help from Xinyu Tan and Hanqing Liu for the preparation of samples for superresolution

imaging. A. P. L. acknowledges support from NSF CMMI-1561794. S. L. V. acknowledges support from R01GM110052.

References

1 A. Diz-Muñoz, D. A. Fletcher and O. D. Weiner, *Trends Cell Biol.*, 2013, **23**, 47–53.
2 S. D. Conner and S. L. Schmid, *Nature*, 2003, **422**, 37–44.
3 H. T. McMahon and E. Boucrot, *Nat. Rev. Mol. Cell Biol.*, 2011, **12**, 517–533.
4 O. Avinoam, M. Schorb, C. J. Beese, J. A. Briggs and M. Kaksonen, *Science*, 2015, **348**, 1369–1372.
5 H. Girao, M.-I. Geli and F.-Z. Idrissi, *FEBS Lett.*, 2008, **582**, 2112–2119.
6 L. M. Fujimoto, R. Roth, J. E. Heuser and S. L. Schmid, *Traffic*, 2000, **1**, 161–171.
7 Å. E. Engqvist-Goldstein and D. G. Drubin, *Annu. Rev. Cell Dev. Biol.*, 2003, **19**, 287–332.
8 S. Boulant, C. Kural, J.-C. Zeeh, F. Ubelmann and T. Kirchhausen, *Nat. Cell Biol.*, 2011, **13**, 1124–1131.
9 T. Hyman, M. Shmuel and Y. Altschuler, *Mol. Biol. Cell*, 2006, **17**, 427–437.
10 S. Aghamohammadzadeh and K. R. Ayscough, *Nat. Cell Biol.*, 2009, **11**, 1039–1042.
11 A. A. Rodal, L. Kozubowski, B. L. Goode, D. G. Drubin and J. H. Hartwig, *Mol. Biol. Cell*, 2005, **16**, 372–384.
12 T. Kishimoto, Y. Sun, C. Buser, J. Liu, A. Michelot and D. G. Drubin, *Proc. Natl. Acad. Sci. U. S. A.*, 2011, **108**, E979–E988.
13 W. Kukulski, M. Schorb, M. Kaksonen and J. A. Briggs, *Cell*, 2012, **150**, 508–520.
14 A. P. Liu, D. Loerke, S. L. Schmid and G. Danuser, *Biophys. J.*, 2009, **97**, 1038–1047.
15 M. Saleem, S. Morlot, A. Hohendahl, J. Manzi, M. Lenz and A. Roux, *Nat. Commun.*, 2015, **6**, 6249.
16 X. Tan, J. Heureaux and A. P. Liu, *Integr. Biol.*, 2015, **7**, 1033–1043.
17 N. Walani, J. Torres and A. Agrawal, *Proc. Natl. Acad. Sci. U. S. A.*, 2015, **112**, E1423–E1432.
18 A. Banerjee, A. Berezhkovskii and R. Nossal, *Biophys. J.*, 2012, **102**, 2725–2730.
19 A. Banerjee, A. Berezhkovskii and R. Nossal, *Phys. Biol.*, 2016, **13**, 016005.
20 N. Cordella, T. J. Lampo, S. Mehraeen and A. J. Spakowitz, *Biophys. J.*, 2014, **106**, 1476–1488.
21 N. Cordella, T. J. Lampo, N. Melosh and A. J. Spakowitz, *Soft Matter*, 2015, **11**, 439–448.
22 S. Mehraeen, N. Cordella, J. S. Yoo and A. J. Spakowitz, *Soft Matter*, 2011, **7**, 8789–8799.
23 P. B. Canham, *J. Theor. Biol.*, 1970, **26**, 61–81.
24 W. Helfrich, *Z. Naturforsch., C: Biochem., Biophys., Biol., Virol.*, 1973, **28**, 693–703.
25 J. T. Jenkins, *SIAM J. Appl. Math.*, 1977, **32**, 755–764.
26 D. J. Steigmann, *Arch. Ration. Mech. Anal.*, 1999, **150**, 127–152.
27 M. Deserno, *Chem. Phys. Lipids*, 2015, **185**, 11–45.
28 H. Duwe, J. Kaes and E. Sackmann, *J. Phys.*, 1990, **51**, 945–961.
29 J. Faucon, M. Mitov, P. Méléard, I. Bivas and P. Bothorel, *J. Phys.*, 1989, **50**, 2389–2414.
30 A. J. Jin, K. Prasad, P. D. Smith, E. M. Lafer and R. Nossal, *Biophys. J.*, 2006, **90**, 3333–3344.
31 A. Agrawal and D. J. Steigmann, *Biomech. Model. Mechanobiol.*, 2009, **8**, 371–379.
32 A. Agrawal and D. J. Steigmann, *Continuum Mech. Thermodyn.*, 2009, **21**, 57–82.
33 H. Gao, W. Shi and L. B. Freund, *Proc. Natl. Acad. Sci. U. S. A.*, 2005, **102**, 9469–9474.
34 J. Liu, M. Kaksonen, D. G. Drubin and G. Oster, *Proc. Natl. Acad. Sci. U. S. A.*, 2006, **103**, 10277–10282.
35 J. Liu, Y. Sun, D. G. Drubin and G. F. Oster, *PLoS Biol.*, 2009, **7**, e1000204.
36 N. J. Agrawal, J. Nukpezah and R. Radhakrishnan, *PLoS Comput. Biol.*, 2010, **6**, e1000926.
37 S. Dmitrieff and F. Nédélec, *PLoS Comput. Biol.*, 2015, **11**, e1004538.
38 D. M. Richards and R. G. Endres, *Proc. Natl. Acad. Sci. U. S. A.*, 2016, **113**, 6113–6118.
39 S. Zhang, H. Gao and G. Bao, *ACS Nano*, 2015, **9**, 8655–8671.
40 J. Agudo-Canalejo and R. Lipowsky, *Biophys. J.*, 2016, **110**, 189a.
41 J. C. Stachowiak, F. M. Brodsky and E. A. Miller, *Nat. Cell Biol.*, 2013, **15**, 1019–1027.
42 F. Hochmuth, J.-Y. Shao, J. Dai and M. P. Sheetz, *Biophys. J.*, 1996, **70**, 358.
43 J. Dai, M. P. Sheetz, X. Wan and C. E. Morris, *J. Neurosci.*, 1998, **18**, 6681–6692.
44 M. B. Stone and S. L. Veatch, *Nat. Commun.*, 2015, **6**, 7347.
45 S. L. Veatch, B. B. Machta, S. A. Shelby, E. N. Chiang, D. A. Holowka and B. A. Baird, *PLoS One*, 2012, **7**, e31457.
46 I. Derényi, F. Jülicher and J. Prost, *Phys. Rev. Lett.*, 2002, **88**, 238101.
47 G. Koster, A. Cacciuto, I. Derényi, D. Frenkel and M. Dogterom, *Phys. Rev. Lett.*, 2005, **94**, 068101.
48 S. Saffarian, E. Cocucci and T. Kirchhausen, *PLoS Biol.*, 2009, **7**, e1000191.
49 T. Kirchhausen, *Trends Cell Biol.*, 2009, **19**, 596–605.
50 M. J. Taylor, D. Perrais and C. J. Merrifield, *PLoS Biol.*, 2011, **9**, e1000604.
51 B. T. Larson, K. A. Sochacki, J. M. Kindem and J. W. Taraska, *Mol. Biol. Cell*, 2014, **25**, 2084–2093.
52 T. Kirchhausen, *Curr. Opin. Struct. Biol.*, 1993, **3**, 182–188.
53 D. Loerke, M. Mettlen, D. Yarar, K. Jaqaman, H. Jaqaman, G. Danuser and S. L. Schmid, *PLoS Biol.*, 2009, **7**, e1000057.
54 A. P. Liu, F. Aguet, G. Danuser and S. L. Schmid, *J. Cell Biol.*, 2010, **191**, 1381–1393.

